Comparative Analysis of Modulation Methods for High-Speed, Low-Inductance Motors

20259066

Keitaro Kawarazaki[1)*], **Taiki Mikami**[1)], **Yuichiro Deguchi**[1)], **Sho Morita**[1)], **Nobukazu Hoshi**[1)]

1)*Tokyo University of Science, Faculty of Science and Technology, Chiba, Japan*

**E-mail: 7323702@ed.tus.ac.jp*

ABSTRACT: This paper examines the impact of modulation methods on the performance characteristics of high-speed and low-inductance motors. Specifically, the attributes of SVPWM (noted for low current ripple), MLDPWM (effective for reducing switching loss), and RSPWM (for suppressing common-mode noise) are compared through simulation for the modulation method. Inverter efficiency maps and current THD maps for rotational speeds up to approximately 50000 min^{-1} were analyzed across these modulation methods. Simulations have revealed clear performance differences among the modulation methods regarding current ripple, inverter efficiency, and common-mode noise for high-speed, low-inductance motor applications.

KEY WORDS: High-speed motor, voltage-source inverter, modulation method, current ripple, common-mode noise.

I. INTRODUCTION

The spread of electric vehicles (EVs) is essential for achieving carbon neutrality, and the number of vehicles with electric drive systems is expected to increase. Currently, high-performance motors for EVs rely on rare earth materials and high-quality electrical steel sheets, both of which face price and supply instability. In addition, a significant challenge in reaching carbon neutrality lies in reducing CO_2 emissions during manufacturing. One promising solution is high-speed motor rotation, enabling high output density and downsizing, conserving resources and reducing manufacturing-related CO_2 emissions. However, operating at high rotational speeds also significantly increases motor iron losses. To address this, coreless motors, which reduce iron losses, have been researched and developed as a high-speed motor solution [1], [2].

Coreless motors tend to exhibit lower inductance and higher winding resistance than traditional motors. In low-inductance motors, the electrical time constant is shorter, causing an increase in current ripple under PWM (pulse width modulation) control due to inverter switching. At high rotational speeds, current ripple further increases because of the higher motor electrical frequencies, which can lead to increased torque ripple and reduced efficiency. A potential approach to mitigate current ripple is to use switching devices capable of high-frequency operation, such as silicon carbide (SiC) power semiconductors; however, there are practical limits to increasing the switching frequency.

Recent trends toward higher-voltage EV batteries, driven by the need to reduce charging time and extend driving range, have also impacted high-speed motor design [3]. At higher speeds, the motor's back electromotive force (EMF) increases, necessitating a higher inverter input voltage. This high voltage amplifies the output voltage variations caused by switching, which, in turn, increases the current ripple. Consequently, higher motor speeds, lower motor inductance, and higher inverter input voltages collectively contribute to increased current ripple in the motor current.

Increased switching losses in voltage-source PWM inverters and higher inverter input voltages also result in common-mode noise, which can impact motor drive systems, leading to issues such as motor shaft voltage buildup and bearing current increase.

Various modulation methods have been proposed to optimize the performance in voltage-source PWM inverters.

Different modulation techniques impact characteristics like current ripple, losses, and common-mode noise [4]. These methods, primarily based on space vector PWM (SVPWM) [5], exhibit varying performance depending on the selected combination of voltage vectors.

For instance, discontinuous PWM (DPWM) [6] minimizes the number of switching cycles to reduce switching losses. Specifically, minimum switching loss DPWM (MLDPWM) [7] is a method that minimizes inverter switching losses by considering the power factor angle. Additionally, reduced common-mode voltage PWM (RCMD-PWM) [4], [8] has been proposed to suppress common-mode noise, while remote state PWM (RSPWM) [4], [8] effectively reduces the common-mode current to zero–although it tends to increase current ripple.

This paper aims to evaluate the effect of the modulation method on high-speed, low-inductance motors driven by high-voltage input PWM inverters. Specifically, this study compares current ripple, inverter efficiency, and common-mode voltage characteristics across different modulation methods. The motor under consideration is a permanent magnet synchronous motor (PMSM) with a maximum electrical frequency of 3.3 kHz (8 poles, 50,000 min^{-1}). Simulations are conducted to compare SVPWM [4], [5], known for its low current ripple; MLDPWM [7], recognized for its high inverter efficiency; and RSPWM [4], [8], which minimizes common-mode current. The SVPWM and RSPWM are implemented on previously proposed methods.

Implementing MLDPWM in high-speed, low-inductance motors requires a tailored strategy due to concerns about modulation wave chattering caused by increased current ripple. Therefore, the next section presents an approach to effectively applying MLDPWM in such motors.

II. MLDPWM FOR HIGH-SPEED, LOW-INDUCTANCE MOTORS

Reference [7] proposes a method for determining the voltage vector to minimum switching losses by considering the motor current and voltage command phase (power factor angle). However, this method only accounts for the fundamental component of the motor's electric angular frequency when determining the motor current and voltage command values. As a result, there is concern that the optimal voltage vector for minimum switching losses may not be accurately determined when harmonic components increases or the output fluctuation occur. Reference [9] proposes MLDPWM-pp (MLDPWM per phase) for four-leg inverters, where the zero voltage vector is determined by the motor current and voltage command value to minimize switching losses. MLDPWM-pp is a method that can pause the switching of the phase with the highest absolute current value among the uvw phases in which switching can be paused. Thus, the switching losses are minimized even when harmonic components increase and output power fluctuates. This paper proposes MLDPWM, which can be used in three-phase inverters based on [9].

First, the calculation method of the duty ratio by SVPWM is explained. For detailed calculations, refer to [10]. The instantaneous output voltage vector diagram is shown in Fig. 1. $\boldsymbol{v_e}$ is the output voltage vector on the α-β coordinate. SVPWM is a method that calculates the three-phase duty ratios such that the sum of the voltage vectors during the switching period outputs $\boldsymbol{v_e}$ based on the voltage command. By labeling the phases u, v, and w in order of the largest duty ratio as a, b, and c, the duty ratios D_a, D_b, and D_c are

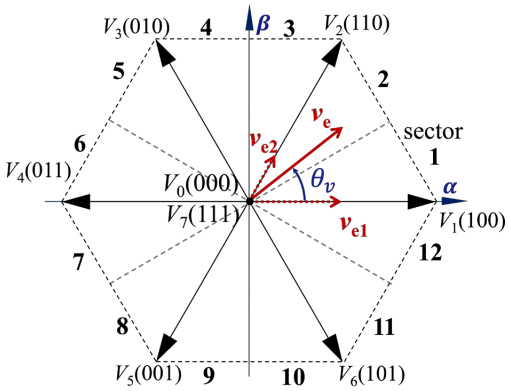

Fig. 1. Definition of output voltage vectors and sectors [10].

expressed by the following equations [10].

$$D_a = k + (1-k)D_{odd} + (1-k)D_{even} \quad (1)$$

$$D_b = k - kD_{odd} + (1-k)D_{even} \quad (2)$$

$$D_c = k - kD_{odd} - kD_{even} \quad (3)$$

Where k is the zero voltage vector ratio, the ratio of odd voltage vectors $\boldsymbol{V_1}$, $\boldsymbol{V_3}$, and $\boldsymbol{V_5}$ is D_{odd}, and the ratio of even voltage vectors $\boldsymbol{V_2}$, $\boldsymbol{V_4}$, and $\boldsymbol{V_6}$ is D_{even}. D_0 and D_7 are the ratios of the two zero voltage vectors V_0 and V_7 in one cycle. The zero voltage vector ratio k is defined as

$$k = \frac{D_7}{D_0 + D_7} \quad (4)$$

$$0 \leq k \leq 1. \quad (5)$$

By setting k to 0 or 1, switching can be paused. In the proposed MLDPWM, k is determined so that switching losses are minimized based on the relationship between motor current and voltage command. One of the three phases can not pause switching, and one of the other two phases is selected to pause switching [11]. Therefore, the switching losses can be minimized by deactivating the switching of the phase with the higher absolute current value out of the two phases for which switching can be deactivated. Table I shows k such that the above conditions are satisfied at all power factors and x, y, and z each represent any of u, v and w phase. Also, i_{mid} [A] and v^*_{mid} [V] are the second-largest current and voltage command values in the uvw phase, respectively.

TABLE I
CONDITIONS FOR VOLTAGE COMMAND VALUES AND CURRENTS WITH A ZERO-VOLTAGE VECTOR RATIO K THAT MINIMIZES SWITCHING LOSSES.

Voltage and current conditions				k
$v_x^* = v_{mid}$	$i_x = i_{mid}$	$i_y^2 \geq i_z^2$	$v_y^* \geq 0$	1
			$v_y^* < 0$	0
		$i_y^2 < i_z^2$	$v_z^* \geq 0$	1
			$v_z^* < 0$	0
	$i_y = i_{mid}$	$v_z^* \geq 0$		1
		$v_z^* < 0$		0
	$i_z = i_{mid}$	$v_y^* \geq 0$		1
		$v_z^* < 0$		0

Furthermore, as mentioned above, the current ripple increases in high-speed, low-inductance motors driven by PWM inverters with high DC input voltages. With the increase in current ripple, there is a concern that the zero-voltage vector ratio k, determined according to Table I, may chatter between 0 and 1. If k chattters between 0 and 1, the switching times increase, and the switching losses also increase. Therefore, this paper introduces a low-pass filter (LPF) at the current value to determine k to implement MLDPWM in the case of increasing current ripple. The LPF is expected to suppress the chattering of k between 0 and 1. Fig. 2 is the control block for the modulation method described above. In this method, the chattering of k is suppressed by introducing a first-order LPF in the dq-axis currents, as shown in Fig. 2. The simulations in the next section show that MLDPWM can be implemented in the case of increased current ripple by the proposed method.

III. SIMULATION

This section presents a simulation-based comparison of common-mode voltage, inverter efficiency maps, and motor current total harmonic distortion (THD) maps for three modulation methods: SVPWM, MLDPWM (proposed method), and RSPWM.

A. Simulation conditions

The simulations were conducted through a co-simulation setup using *MATLAB/Simulink* and *PLECS*. *MATLAB/Simulink* was utilized for control calculations, while *PLECS* analyzed switching device losses and the

TABLE II
MOTOR PARAMETERS OF IPMSM USED IN SIMULATION.

Motor type	IPMSM
Number of pole pairs	4
d-axis inductance L_d	60 μH
q-axis inductance L_q	90 μH
Permanent magnet flux linkage ψ_a	0.027 Wb
Winding resistance R_a	0.352 Ω
Limited torque	15 Nm
Limited Motor speed	50000 min^{-1}

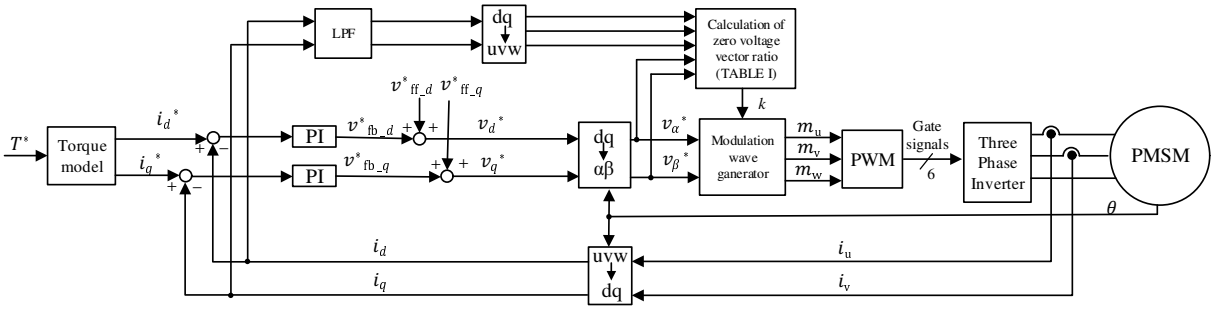

Fig. 2. Control block diagram of MLDPWM for high-speed, low-inductance motor.

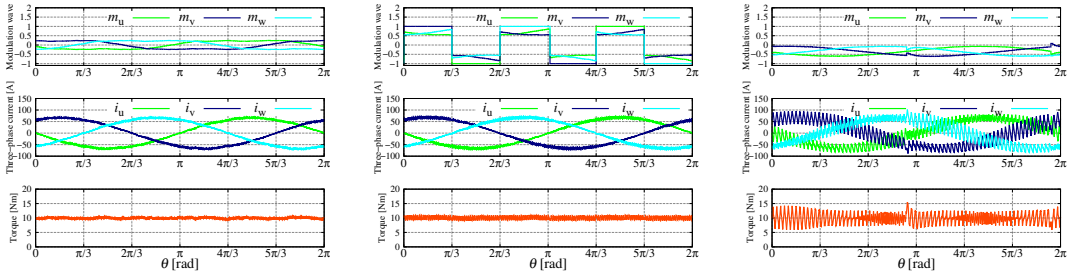

(a) SVPWM. (b) MLDPWM. (c) RSPWM.

Fig. 3. Modulation waveforms, three-phase currents, and torque waveforms for each modulation method.

motor model. The motor parameters used in the simulation are listed in Table II. The inverter input voltage $V_{\rm dc}$ was set to 1000 V, and the switching frequency was 100 kHz. For the switching devices analysis, publicly available "*Thermal Semiconductor Models for PLECS*" models were used.

B. Simulation results

Fig. 3 shows the waveforms of modulation waves m_{uvw}, three-phase currents i_{uvw} [A], and torque for SVPWM, MLDPWM, and RSPWM obtained by the simulations at 10000 $\rm min^{-1}$ and 10 Nm. The MLDPWM modulation waveforms in Fig. 3(b) are clamped at -1 or 1, meaning no switching occurs at these extremes, which helps reduce switching losses. In MLDPWM, the phase with the larger current magnitude is clamped to minimize further switching losses, though this does increase the current ripple compared to SVPWM. The RSPWM current waveforms of Fig. 3(c) show greater current ripple, especially relative to the other modulation methods.

Next, the requirement for LPF in Fig. 2 is shown for MLDPWM with increased current ripple. Fig. 4 shows the u-phase modulation wave, u-phase current, and torque waveforms with and without LPF at 10000 $\rm min^{-1}$ and 5 Nm. The time constant of the LPF was set to 20 μs. In the method without LPF, the modulation wave is chattering. The current and torque ripple increased accordingly. In contrast, with the LPF shown in Fig. 2, the chattering of the modulation wave is suppressed. Comparing the switching losses, 315 W with LPF and 612 W without LPF, the proposed method also suppresses the switching losses. Fig. 5 shows the power factor angle characteristics of the switching losses of DPWM [6] and MLDPWM. The switching loss improvement rate (SLI) [%] is defined as

$$SLI = \frac{P_S - P_A}{P_S} * 100, \tag{6}$$

where P_S [W] is the switching loss of SVPWM without switching pause and P_A is the switching loss of any modulation method. From Fig. 5, MLDPWM shows an improved *SLI* at all power factor angles despite having the same switching pause period as DWPM.

The analysis results of the common-mode voltage v_{cm} [V] are shown next. Common-mode noise arises from common-mode current i_{cm} [A], which flows through the stray capacitance C_{CM} [F] due to fluctuations in the voltage v_{uo}, v_{uo}, and v_{uo} between the inverter terminal and ground as shown in Fig. 6. The common-mode current i_{cm} is calculated as follows:

$$i_{\mathrm{cm}} = 3C_{\mathrm{CM}}\frac{dv_{\mathrm{cm}}}{dt},\ v_{\mathrm{cm}} = \frac{v_{uo}+v_{vo}+v_{wo}}{3}. \tag{7}$$

As shown in Fig. 7, the number of common-mode voltage v_{cm} transitions per switching cycle is six for SVPWM, four for MLDPWM, and zero for RSPWM. This means that RSPWM generates no common-mode noise. In contrast, SVPWM has higher common-mode voltage fluctuations than MLDPWM due to more frequent v_{cm} changes. Consequently, i_{cm} = 0 A for RSPWM. These figures indicate a trade-off between the common-mode noise and current ripple magnitude across the three modulation methods.

Finally, Figs. 8 and 9 present the inverter efficiency maps and THD maps of u-phase current of each modulation method. The maps for RSPWM are narrower due to its lower voltage utilization than SVPWM and MLDPWM. The MLDPWM inverter efficiency map shows higher efficiency across all operating points than SVPWM and RSPWM, as MLDPWM minimizes switching losses. Comparing current

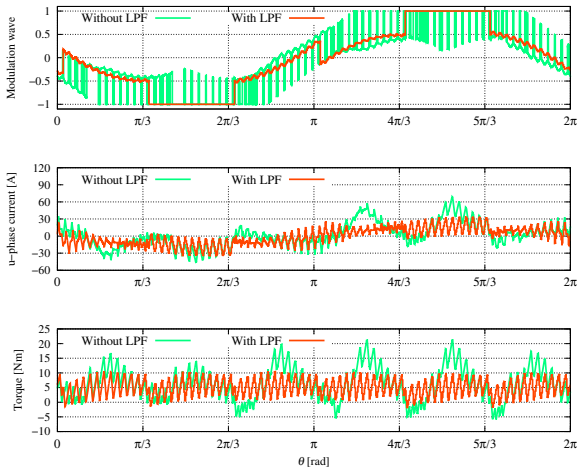

Fig. 4. Waveforms of modulation waves, u-phase currents and torques with and without LPF in the proposed method.

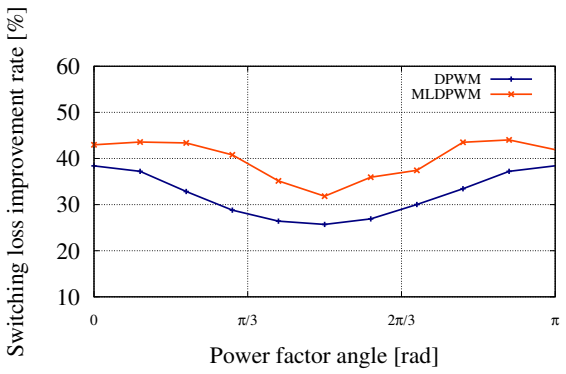

Fig. 5. Switching loss improvement rate for DPWM and MLDPWM.

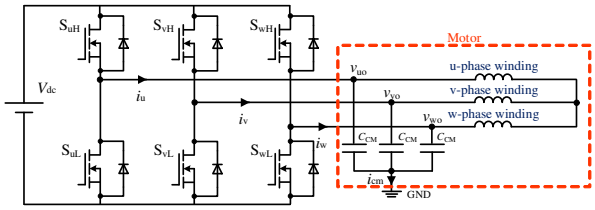

Fig. 6. Motor drive systems considering leakage currents.

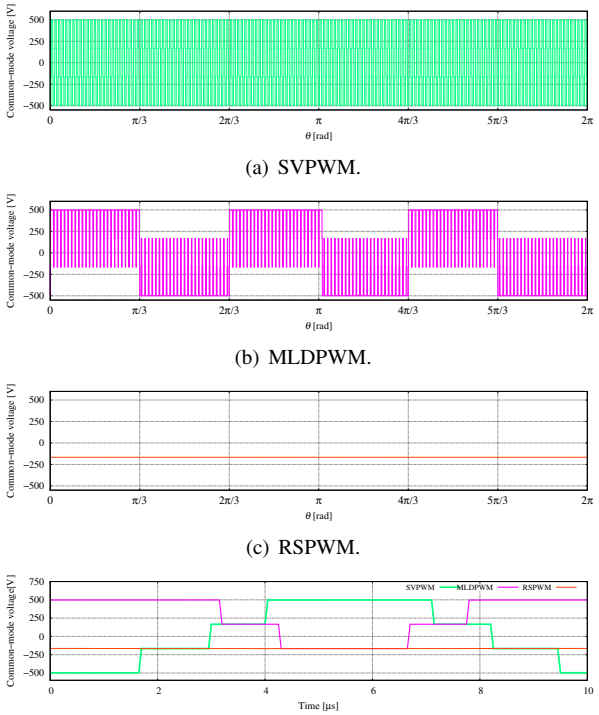

Fig. 7. Common-mode voltage characteristics for each modulation method.

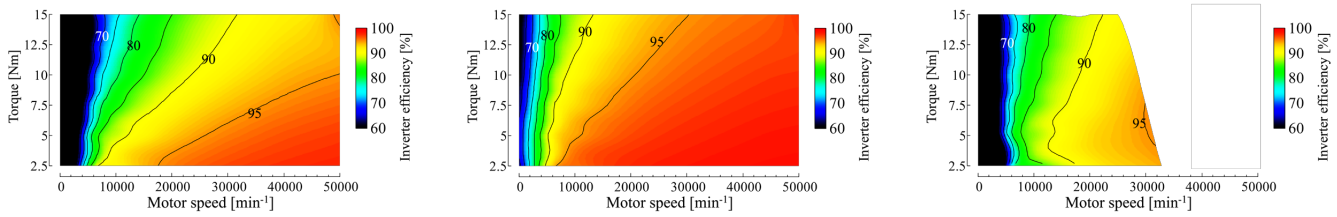

(a) SVPWM. (b) MLDPWM. (c) RSPWM.

Fig. 8. Inverter efficiency maps.

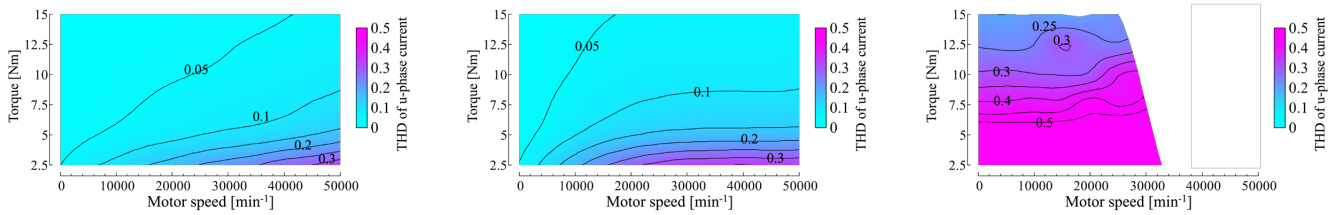

(a) SVPWM. (b) MLDPWM. (c) RSPWM.

Fig. 9. THD maps of u-phase current for each modulation method.

THD maps, RSPWM performs the worst; its THD exceeds 0.25 at all operating points with a low-inductance motor, and some low-torque areas exceed a THD of 1.0. The increased current ripple in RSPWM can lead to control instability and decreased motor efficiency. The SVPWM maintains a lower current THD than MLDPWM across all operating points, although MLDPWM's THD is still lower than RSPWM.

IV. Conclusion

This paper compared the characteristics of SVPWM, MLDPWM, and RSPWM methods for high-speed, low-inductance motors. Additionally, to suppress chattering that can increase switching losses, this paper proposes an implementation method of MLDPWM for high-speed, low-inductance motors. The results showed that the current ripple performance, ordered from highest to lowest, is SVPWM, followed by MLDPWM, with RSPWM exhibiting the lowest performance, particularly under high-speed conditions. In terms of inverter efficiency, MLDPWM provided the highest efficiency due to minimized switching losses. For common-mode noise, RSPWM was the most effective, followed by MLDPWM and then SVPWM; notably, RSPWM entirely eliminated common-mode noise.

These findings suggest that RSPWM may generate excessive current ripple for high-speed, low-inductance motors under the conditions examined in this study. SVPWM is likely more suitable for low-torque applications where reducing current THD is important, while MLDPWM is advantageous for high-torque scenarios to mitigate losses.

Acknowledgment

This paper is based on results obtained from a subcontract from Transmission Research Association for Mobility Innovation (TRAMI) as part of the New Energy and Industrial Technology Development Organization (NEDO) Feasibility Study Program on Energy and New Environmental Technology / Resource saving of electric drive system for automobiles by ultra-high rotation of e-motor. (JPNP14004).

References

[1] S. Neethu, S.P. Nikam, A. K. Wankhede, Saumitra Pal and B.G. Fernandes, "High Speed Coreless Axial Flux Permanent Magnet Motor with Printed Circuit Board Winding", *IEEE Trans. on Industry Applications*, vol. 55, no. 22, pp. 1954-1962, Mar-April 2019.

[2] T. Kosaka, C. Higashihama, T. Ishihara, H. Matsumori and N. Matsui, “Design Study on Light-weight Quasi-coreless SPMSM using CFRP, Small Amount of SMC Core and Aluminum Winding,” *2023 11th International Conference on Power Electronics and ECCE Asia (ICPE 2023 - ECCE Asia)*, Jeju Island, Korea, Republic of, 2023, pp. 2338-2343.

[3] I. Aghabali, J. Bauman, P. J. Kollmeyer, Y. Wang, B. Bilgin and A. Emadi, “800-V Electric Vehicle Powertrains: Review and Analysis of Benefits, Challenges, and Future Trends,” *IEEE Transactions on Transportation Electrification*, vol. 7, no. 3, pp. 927-948, Sept. 2021. Winding,” *2023 11th International Conference on Power Electronics and ECCE Asia (ICPE 2023 - ECCE Asia)*, Jeju Island, Korea, Republic of, 2023, pp. 2338-2343.

[4] A. M. Hava and E. Ün, “Performance Analysis of Reduced Common-Mode Voltage PWM Methods and Comparison With Standard PWM Methods for Three-Phase Voltage-Source Inverters,” *IEEE Transactions on Power Electronics*, vol. 24, no. 1, pp. 241-252, Jan. 2009.

[5] H. W. van der Broeck, H. -C. Skudelny and G. V. Stanke, “Analysis and realization of a pulsewidth modulator based on voltage space vectors”, *IEEE Transactions on Industry Applications*, Vol. 24, No. 1, pp. 142-150, 1988.

[6] K. Taniguchi, Y. Ogino and H. Irie, “PWM technique for power MOSFET inverter”, *IEEE Transactions on Power Electronics*, Vol. 3, No. 3, pp. 328-334, 1988.

[7] Dae-Woong Chung and S. -K. Sul, “Minimum-loss strategy for three-phase PWM rectifier,” *IEEE Transactions on Industrial Electronics*, vol. 46, no. 3, pp. 517-526, June 1999.

[8] M. Cacciato, A. Consoli, G. Scarcella and A. Testa, “Reduction of common-mode currents in PWM inverter motor drives,” *IEEE Transactions on Industry Applications*, vol. 35, no. 2, pp. 469-476, March-April 1999.

[9] S. Y. Kim, S. G. Song and S. J. Park, “Minimum Loss Discontinuous Pulse-Width Modulation Per Phase Method for Three-Phase Four-Leg Inverter,” *IEEE Access*, vol. 8, pp. 122923-122936, 2020.

[10] K. Kawarazaki and N. Hoshi, “A novel modulation method for three-phase inverter with pausable switching during arbitrary periods in an arbitrary phase,” 2023 11th *International Conference on Power Electronics and ECCE Asia (ICPE 2023 - ECCE Asia)*, Jeju Island, Korea, pp. 3029-3036, 2023.

[11] K. Kawarazaki and N. Hoshi, “Space Vector Modulation with Flexible Switching Pause Period Function for Three-Phase PMSM Drive Inverters,” *2024 27th International Conference on Electrical Machines and Systems (ICEMS)*, Fukuoka, Japan, 2024.